Energy Conversion and Management 286 (2023) 117052

Contents lists available at ScienceDirect

Energy Conversion and Management

journal homepage: www.elsevier.com/locate/enconman

Effect of diethyl ether addition to waste cooking oil biodiesel on the combustion and emission characteristics of a swirl-stabilized premixed flame

Radwan M. EL-Zohairy [1], Ahmed S. Attia [1], A.S. Huzayyin, Ahmed I. EL-Seesy [*]

Mechanical Engineering Department, Benha Faculty of Engineering, Benha University, 13512 Benha, Qalubia, Egypt

ARTICLE INFO

Keywords:
Diethyl ether
Waste cooking oil biodiesel
Transesterification
Swirl-stabilized premixed combustion
Flame characterization
Emission aspects

ABSTRACT

Waste cooking oil biodiesel is a promising alternative to diesel and jet fuels. However, the challenge of using waste cooking oil biodiesel is its higher viscosity and lower volatility than diesel fuel, which hinder its spray and atomization from achieving diesel levels. These drawbacks can be enhanced by adding a less viscous fuel like diethyl ether. Thus, an experimental approach has been performed to investigate the effect of diethyl ether addition to waste cooking oil biodiesel in the lean pre-vaporized premixed system. Test fuels considered in this study are B20 (20% biodiesel + 80% Jet A-1), B20D10 (20% biodiesel + 10% diethyl ether + 70% Jet A-1), B20D30 (20% biodiesel + 30% diethyl ether + 50% Jet A-1) as well as pure Jet A-1. These blends are applied in the lean pre-vaporized premixed system with preheated air at 350 ℃ at a fixed equivalence ratio of 0.85 (lean condition). Results showed a 68, 38.4, 14.5, and 43.4% decrease in CO, NO_x, CO_2, and UHC emissions, respectively, for the B20D30 blend, compared with pure Jet A-1 fuel at the combustor exit, while the B20D10 blend indicated a 15.8, 8.9, 6.17, and 51.4% drop in CO, NO_x, CO_2, and UHC levels, correspondingly. Jet A-1 achieved a higher maximum temperature than those for other blends. The B20 blend revealed a relative variation in flame temperature distribution, while diethyl ether blends shared a similar temperature distribution compared with Jet A-1. Generally, B20D10 and B20D30 blends had the ability to reduce emission levels. Overall, it can be concluded that the recommended diethyl ether blending ratio is 30%, regarding emission levels and flame temperature profile.

1. Introduction

Developing non-petroleum fuels for engines, especially aircraft engines, has a great international interest due to the rising petroleum prices and the rapidly increasing environmental threat of exhaust emissions and global warming [1]. Aircraft engines share around 3% of global warming emissions, and they are predicted to contribute further [2]. Due to these environmental threats and fossil fuel depletion, renewable alternative aviation fuels are gaining significant interest [2]. Biodiesel has recently attracted much attention because it is environmentally friendly, non-toxic, biodegradable, and can be produced using various renewable resources [3]. Habib et al. [4] tested soybean, recycled rapeseed, canola, and hog-fat biodiesel, and their blends with Jet A-1 in a gas turbine and found a drop in static thrust, specific fuel consumption, NO_x, and CO emissions compared with Jet A-1.

Essentially, three generations of feedstocks are utilized to produce biodiesel: the 1st, 2nd, and 3rd generations [5]. The 1st generation biodiesel feedstocks include food oils such as rapeseed, palm, soybean, and castor [5]. However, food oils negatively affect food security, including price increases for food and feed supplies due to increased demand [6]. As a result, scientists turned to the oils of non-food crops, such as jatropha and jojoba, which are considered 2nd generation feedstocks for biodiesel [5]. The 2nd generation feedstocks have no food issues and may be cultivated in the desert and irrigated with wastewater, but are grown by only a few farmers. The 3rd generation feedstocks overcome the problems of earlier generations, such as food security, costs, and availability. Thus, the 3rd generation feedstocks, including waste cooking oil (WCO), fat chicken oil, fish oil, and microalgae, are widely used for biodiesel production [5].

Since feedstocks comprise about 70–80% of the total cost of biodiesel production, using widely available and cheap feedstock could reduce the

* Corresponding author.
E-mail address: ahmed.elsysy@bhit.bu.edu.eg (A.I. EL-Seesy).
[1] Co-first author: They have an equal contribution and are considered as one author.

https://doi.org/10.1016/j.enconman.2023.117052
Received 2 February 2023; Received in revised form 2 April 2023; Accepted 12 April 2023
Available online 24 April 2023

Nomenclatures

Abbreviation	Definition
B_α	Blend contains α% biodiesel and (100-α) % Jet A-1
BαDγ	Blend contains α% biodiesel, γ% diethyl ether, and 100-(α + γ) % Jet A-1
CN	Cetane number
CO	Carbon monoxide
CO_2	Carbon dioxide
DAQ	Data acquisition
DEE	Diethyl ether
EA	Elemental analyzer
JOME	Jojoba oil methyl ester
KOH	Potassium hydroxide
LHV	Lower heating value
LPP	Lean pre-vaporized premixed
NO_x	Nitrogen oxides
SMD	Sauter mean diameter
SN	Swirl number
STP	Spray tip penetration
SCA	Spray cone angle
SPA	Spray projected area
TGA	Thermogravimetric analysis
UHC	Unburned hydrocarbons
UNOSSC	United Nations Office for South-South Cooperation
WCO	Waste cooking oil
WCOME	Waste cooking oil methyl ester
Symbol	Definition [Unit]
ΔP_1	Pressure drop across the injector nozzle [Pa]
EI_i	Emission index [-]
$\dot{m}$	Fuel mass flow rate [Kg/s]
MW_f	Molecular weights of the fuel [kg/kmol]
MW_i	Molecular weights of species i [kg/kmol]
PF	Pattern factor [-]
R	Radial location from the burner centerline (mm) [mm]
T_f	Flame temperature [K]
X_c	Number of moles of carbon in one mole of fuel [mol]
Z	Vertical location above the burner tip [mm]
μ	Dynamic viscosity [Pa.s]
ρ_a	Surrounding air density [Kg/m^3]
σ	Surface tension [N/m]
φ	Equivalence ratio [-]
χ_i	Mole fractions of species i [-]

price of biodiesel production [7]. One of the available and affordable feedstocks for biodiesel is waste cooking oil, which can reduce the global pressure on edible resources caused by global conflicts, especially the Ukraine-Russia war [8]. Recent studies have shown that waste cooking oil can be converted into various products with additional value, including surfactants, biolubricants, polyurethane, grease, plastics, and bio-asphalt [9], but the current study focuses on biodiesel production.

According to the 2017 United Nations Office for South-South Cooperation (UNOSSC) report, an estimated 500,000 tons of waste cooking oil are available annually in Egypt from many sources, like food factories, restaurants, hotels, and homes [10]. Reusing cooking oil in food production has been shown to raise the risk of cancer and cardiovascular disease due to its oxidation and poisonous components [11]. About 90% of homes discharge their waste cooking oil into the drains. Instead of reusing cooking oil in food production or polluting the environment, it can be used as a biodiesel feedstock. The idea of exploiting waste cooking oil for biodiesel production in Egypt started in 2013 [10]. Li et al. [12] observed that waste cooking oil biodiesel reduced NO_x, CO, and UHC levels emitted from a radial swirler gas turbine combustor in the lean combustion range.

On the other hand, biodiesel has some drawbacks, such as higher viscosity, higher surface tension, and lower volatility than diesel fuel [13]. Also, the spraying and atomization of biodiesel can not meet diesel levels [14]. This could lead to poor performance in forming a combustible mixture [14]. Agarwal & Chaudhury and Wang et al. [15,16] investigated the spray characteristics of biodiesel blended with diesel and observed a greater spray tip penetration (STP) length, less air entrainment, and a relatively large sauter mean diameter (SMD), which deteriorates mixture formation. In addition, biodiesel worsens in cold weather due to its poor cold flow characteristics [17]. Due to these drawbacks, biodiesel is usually blended with diesel at no more than a 20% mixing ratio. Therefore, it is suggested that adding less viscous fuel like diethyl ether (DEE) or dibutyl ether (DBE) to biodiesel can improve its viscosity, density, and surface tension, thus compensating for its poor cold flow characteristics [18]. Also, DEE is considered an oxygenated additive, which can help further cut exhaust emissions when blended with biodiesel [1].

Diethyl ether $(C_2H_5)_2O$ can be prepared by dehydrating ethanol using solid acid catalysts and is regarded as an attractive biofuel [19]. DEE has a high vapor pressure (around 110.2 kPa at 293 K), which improves the atomization process and mixture formation and is desirable for engine starting, particularly at cold temperatures [17]. Also, DEE has a higher evaporation latent heat than diesel and biodiesel. Thus, mixing DEE with either diesel or biodiesel will decrease the peak temperature in the combustion process, which is predicted to diminish NO_x formation. The recent investigations about ether fuels in external combustion are summarised in Table 1.

Zhan et al. [14] investigated the influences of DEE and ethanol addition to diesel–biodiesel blends in a constant volume chamber using a common rail injector under high pressure. They concluded that mixing DEE with diesel–biodiesel blends accelerated secondary small droplet formation, which enhanced the atomization process of diesel–biodiesel blends. Due to DEE's lower surface tension and dynamic viscosity than diesel and biodiesel, the fuel ligaments and droplets break up quickly into finer droplets. Tran et al. [19] investigated the impacts of utilizing DEE as a fuel additive and as a neat biofuel on pollutant formation and flame structure in premixed flames and found that hydrocarbon species were significantly reduced in the flames containing DEE. Guan et al. [20] studied the effects of dibutyl ether (DBE) addition to soybean biodiesel on macroscopic and microscopic spray characteristics in a constant volume combustion chamber with a common-rail fuel injection system. The results showed that DBE improved biodiesel atomization by reducing SMD due to its lower viscosity, density, and surface tension. Gao et al. [21] also investigated the effects of adding DBE to biodiesel in a laminar diffusion flame using a constant volume combustion chamber with a blending ratio range of DBE from 0 to 40%. The experiment results showed that adding DBE led to a reduction in soot formation. Fu et al. [18] studied the spray characteristics of soybean biodiesel blended with di-n-butyl ether at mixing ratios of 15 and 30% in a constant-volume combustion chamber. They observed that the STP of the blends was shortened, and the spray cone angle was increased with the di-n-butyl ether addition.

Regarding the previous works, WCO biodiesel has several merits, including availability, being eco-friendly due to its recycling, and providing renewable energy with less pollution, cheap collection, and reduced waste management costs. However, its viscosity and volatility are considered the main drawbacks, hindering its use at high proportions with Jet A-1 fuel. Meanwhile, a lean pre-vaporized premixed (LPP) system is regarded as a promising method to reach low-temperature techniques and simulate the gas turbine application.

Table 1
Previous studies that researched how ether fuels affect biodiesel.

Ref.	Base Fuel	Additive Type	Blending ratio	Combustion mode	Results
[14]	Diesel (D)	Soybean biodiesel (B), Ethanol (E), Diethyl ether (DEE)	• D100 • B20 • B16E20 • B16DEE20	Spray combustion	• Biodiesel increased SMD. • DEE increased SMD. • DEE improved fuel atomization.
[19]	Butane (BU)	Butane (BU), Diethyl ether (DEE), Butanol (BUOH),	• BU • DEE • BU/DEE • BUOH • BUOH/DEE • BU/BUOH	Laminar premixed flame	• DEE reduced the soot formation. • Oxygenated fuel flames produce less toxic carbonyls, such as formaldehyde and acetaldehyde.
[20]	Diesel (D)	Soybean biodiesel (B), n-butyl ether (DBE).	• Diesel • B100 • DBE100 • DBE15 • DBE30	Spray combustion	• Biodiesel had lower SCA and SPA than blended fuels. • Biodiesel spray tended to larger droplets, while DBE30 spray had an increased tendency to smaller droplets. • DBE significantly improved the spray and atomization of biodiesel.
[21]	Methyl decanoate (MD)	Dibutyl ether (DBE).	• MD100 • DBE10 • DBE20 • DBE30 • DBE40	Co-flow diffusion flame	• DBE decreased soot formation.
[18]	Diesel (D)	Soybean biodiesel (B) Di-n-butyl ether (E)	• D100 • B100 • B85E15 • B70E30	Spray combustion	• The blends' STP was shortened. • SCA was increased.
[22]	dimethyl ether	———	———	Co-flow flame	• The liftoff heights increased linearly with the increase of central jet flow. • The liftoff heights were inversely proportional to the CH4 equivalence ratio.
[23]	Diesel (D)	Dimethyl ether (DME)	• D100 • DME5 • DME10 • DME100	Spray combustion	• Increasing the mass fraction of DME in the blend increased the spray angle, so it had good evaporation properties. • Spray penetration length decreased with increased DME blending ratios.

WCO was transesterified into waste cooking oil methyl ester (WCOME) in a single-step process using methanol as an alcohol and KOH as a catalyst. Ethers fuel like DEE was used as fuel additives to enhance biodiesel application in external combustion systems, and they were recommended by Zhan et al. [14] and Tran et al. [19], who investigated the effects of adding DEE to biodiesel on the spray characteristics and

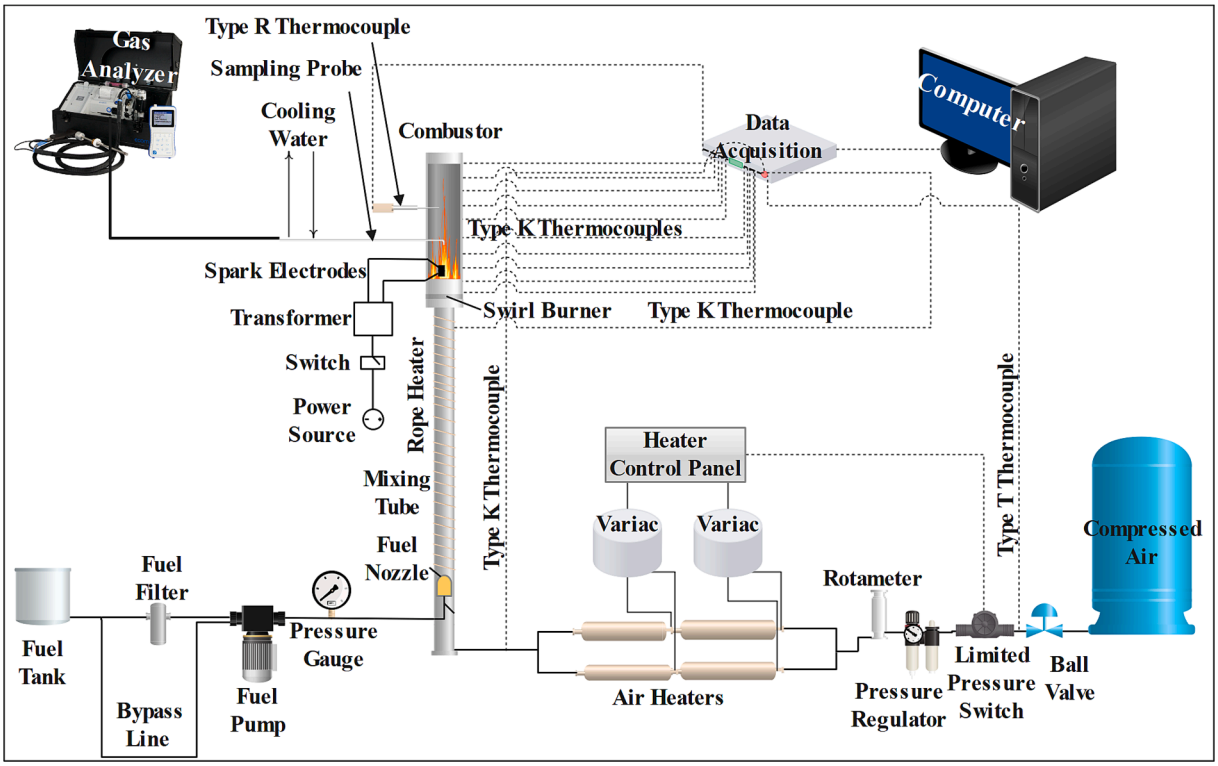

Fig. 1. A schematic diagram of the test rig.

premixed flames. Regarding the best authors of knowledge, the impacts of adding DEE as an additive to the WCO biodiesel/Jet A-1 blend have not been studied yet. To meet this gap, the current study attempts to improve the application of WCO biodiesel in the LPP system by utilizing DEE as a fuel additive. Two proportions of DEE are applied to the WCOME-Jet A-1 blend: 10 and 30% by volume. Finally, the fuel blends were tested for combustion and emission characteristics and compared with Jet A-1.

2. Experimental setup and procedures

The setup and test methods for the experiment are described in this section. The components of the test rig are illustrated in the first subsection. Then the test fuels' preparation, with their physical and chemical properties, are discussed in the second subsection. Finally, the third and fourth subsections describe the testing procedures and measuring techniques.

2.1. Experimental setup

A test rig was established and equipped with the required measuring instruments to study the combustion characteristics of the DEE-WCOME-Jet A-1 fuel blends utilizing the LPP combustion approach, as shown in Fig. 1. This testing facility is described as follows:

A screw compressor compresses air into a 2 m^3 accumulator tank with a pressure-regulating valve fitted on the airline. The airflow rate is measured with a glass rotameter with a flow range of 1.7 to 27 m^3/h. A pressure gauge and a thermocouple type T (connected to a Data Acquisition Card (DAQ) system) are used to monitor air pressure and temperature.

Four electric heaters are used to heat the air before it enters the mixing tube through two parallel paths. Each path has two series of inline heaters, one with a load of 1200 W and the other with a load of 750 W. Two variable AC transformers control the heating system by varying the voltage supplied to the heaters to get the desired air temperature. A type K thermocouple measures the output air temperature.

The fuel is supplied from a 2 L beaker and is delivered by a pump to the fuel nozzle, which atomizes fuel continuously under high pressure in the mixing tube. The fuel nozzle is a single-hole design with a flow rate of 1.9 L/h, a solid spray pattern, and an angle of 45°. The atomized fuel is mixed with the preheated air through the steel pipe mixing tube. A 25-mm-thick ceramic thermal insulation layer covers the mixing tube to minimize heat losses to the ambient. Moreover, an extra rope heater is fitted along the mixing tube to maintain temperature.

The experiments were performed using a radial swirl burner with eight straight vanes, an angle of 45°, and a swirl number (SN) equal to 0.55. The combustion chamber is 150 mm in diameter and 500 mm in length, while the burner is 16.1 mm in diameter. Temperatures and species concentrations are measured along the flame through five measuring holes of 10 mm diameter in the combustor's upper section and a 164-mm-long, 10-mm-wide groove at the bottom. The combustor is also equipped with 10 welded nuts, and 10 type K bolt thermocouples are fitted to measure the wall temperatures simultaneously.

Two electrodes set on a ceramic base are wired to the spark ignition transformer via high-voltage wire, generating 2 × 12 kV at 30 mA to ignite the premixed fuel–air mixture.

2.2. Test fuels

Commercial Jet A-1, waste cooking oil biodiesel, and DEE were utilized to study the combustion and emission characteristics under different blending ratios. The Jet A-1 was purchased from Misr Petroleum Company, and DEE was obtained locally, whereas biodiesel was prepared in the biodiesel lab from the collected residential waste cooking oil via a transesterification process. In this work, the optimal conditions proposed by Attia and Hassaneen [24] were adopted, as presented in Table 2.

The following steps were followed to produce biodiesel:

i. Weighing 1 L of raw oil on the electronic digital scale and heating it to 110℃ for 10 min to get the oil free of moisture, then letting it cool to 60℃.
ii. Preparing the methoxide solution by adding Potassium hydroxide (KOH) flakes with 1% of the weight of the raw oil to 330 ml of methanol, then mixing them well by using the magnetic stirrer for 5 min.
iii. Carefully pouring the methoxide solution into the oil beaker and maintain the mixture temperature at 60℃ while covering the beaker with stretched plastic to prevent any vaporized methanol from escaping from the beaker.
iv. Operating the rotor–stator homogenizer at 12,000 rpm for 1.5 h.
v. Pouring the mixture into the separating funnel for one day to ensure complete glycerol separation from esterified oil.
vi. The bottom layer of glycerol is removed while the top layer of biodiesel is washed.
vii. Bubble-washing the top layer with warm water several times to remove any residual glycerin and soap until clear water is observed.
viii. Collecting the washed biodiesel from the separating funnel and heating it to 105 ± 3℃ for about 10 min to evaporate any residual water and obtain the WCOME final product.

A thermogravimetric analysis (TGA), gas chromatography-mass spectrometry, and Fourier transform infrared spectroscopy were used to evaluate the produced biodiesel, as shown in Fig. 2, Fig. 3, and Table 3. Fig. 2 illustrates the biodiesel starting to vaporize gradually at 200 °C and completely evaporating at about 450℃ with no residuals, compared with 500℃ for raw oil. Thus, the transesterification process improved the volatility of oil. The deflection in the two curves represents the transition from raw oil into biodiesel. By identifying FAME groups in the spectrum, Fourier transform infrared spectroscopy (FTIR) has proven effective in ensuring the transformation of raw oil into biodiesel [25]. Fig. 3 indicates the transformation of WCO to WCOME. This is due to the presence of grouping indicative of methyl ester (CO-O-CH3) at 1452 (1/m), ester stretch (C = O) at 1741 (1/m), methyl (–CH3) at 2935 and 2850 (1/cm), and hydroxyl (–OH) at 3500–3000 (1/cm) [26]. GC–MS results (using a Shimadzu QP2010Ultra equipped with a 5MS column) are presented in Table 3. Methyl tetradecanoate, hexadecanoic acid-methyl ester, 9-octadecenoic acid-methyl ester, and methyl stearate are the four most abundant FAMEs in this table, and they all have unique retention times and fragmentation patterns.

The basic physical and chemical properties of the pure blending stocks are shown in Table 4. A METTLER TOLEDO DM40 density meter was used to determine the fuel density at 20℃, while viscosity was measured by using a pre-calibrated Ostwald viscometer at 40℃. The flash point of fuels was measured by using a SETA PM-93 automated flash point tester according to standard ASTM D93. The carbon, nitrogen, hydrogen, and sulfur mass fractions in fuels were analyzed by using the EuroVector EA3000 CHNS-O Elemental Analyzer. The lower calorific value of fuels was calculated according to El-Maghraby's formula [27], while the surface tension was calculated according to Saxena et al.'s formula [28]. As shown in Table 4, biodiesel has a greater specific gravity and kinematic viscosity than Jet A-1, while the specific gravity, viscosity, and surface tension of DEE are the lowest among the fuels. Biodiesel's calorific value is 8.7% lower than diesel's but 8.5% greater than that of DEE. Biodiesel has the greatest flash point. The cetane number (CN) of DEE is more than double that of biodiesel. DEE has an oxygen content of 21.6%, while biodiesel has only 11.3%. Increasing the DEE percentage in the blends improves the fuel's oxygen content, cetane number, kinematic viscosity, density, and lower heating value.

Biodiesel was mixed with Jet A-1 at a blending ratio of 20 % (B20), then two blends were prepared with two volume blending ratios of DEE:

Table 2
Transesterification reaction conditions.

Alcohol	Molar ratio	Catalyst	Catalyst Concentration	Mixing technique	Mixing period	Reaction temperature
Methanol	6:1	KOH	1% of the oil weight	Mechanical stirring	1.5 h	60℃

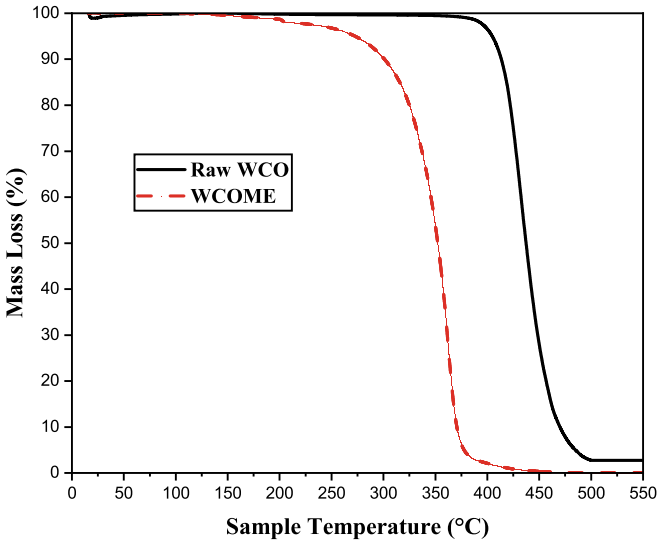

Fig. 2. TGA of raw WCO vs. WCO Biodiesel.

10% DEE and 20% biodiesel with 70% Jet A-1 (B20D10) and 30% DEE and 20% biodiesel with 50% Jet A-1 (B20D30). The mixing ratios of the different blends are shown in Table 5. A digital homogenizer, IKA ULTRA-TURRAX® T18, was utilized to obtain homogenous mixtures.

The prepared samples were evaluated based on their physical and chemical characteristics, such as density at 20℃, viscosity at 40℃, flash point, elemental analysis, heating value, and thermogravimetric analysis, as shown in Table 6.

Also, a thermogravimetric analysis (TGA) was performed for the tested fuels to indicate the volatility of the fuels so that the proper preheated temperature could be chosen to achieve the vaporization of the fuel. The thermogravimetric analysis measures how much and how quickly a material's mass changes as a function of temperature. A Labsys Evo-Setaram analyzer was utilized to do these tests. The TGA for the tested fuels is shown in Fig. 4. The figure illustrates that Jet A-1 starts to evaporate at 120℃ and completes its evaporation at 250℃. While the B20 blend, on the other hand, has a similar volatility profile as Jet A-1, only up to 50%, but with complete evaporation at 340 °C. Once DEE was added, the B20D10 and B20D30 blends started to evaporate at approximately 34℃ and completed evaporation at 340℃. Since fuel

Table 3
Composition and chemical formula of WCO biodiesel's FAME.

Retention time (min)	Component	Symbol	Structure	Formula
9.75	Methyl tetradecanoate	C16:1		$C_{15}H_{30}O_2$
11.78	Hexadecanoic acid, methylester	C16:1		$C_{17}H_{34}O_2$
13.68	9-Octadecenoic acid, methyl	C18:1		$C_{19}H_{36}O$
13.88	Methyl stearate	C18:1		$C_{19}H_{38}O_2$

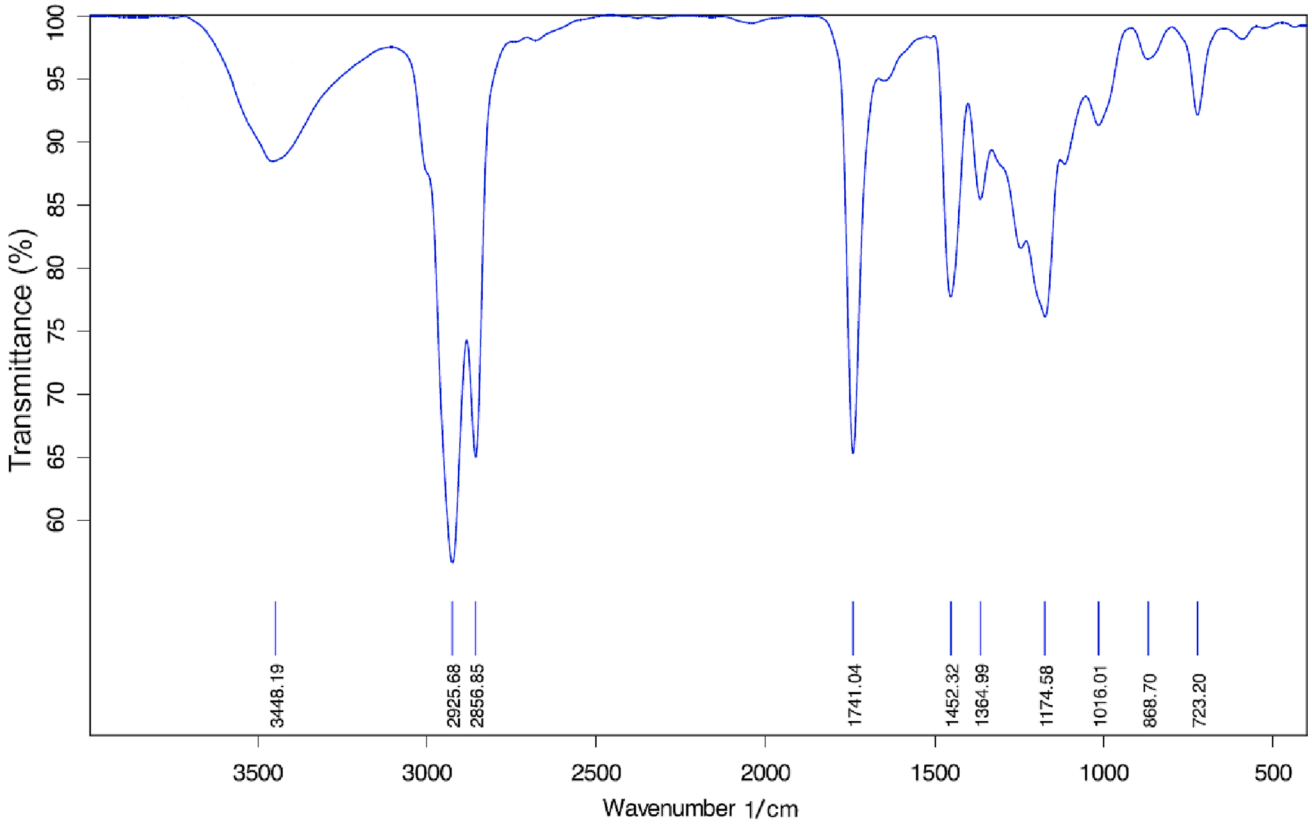

Fig. 3. FT-IR spectrum of WCOME.

Table 4
Properties of Jet A-1, WCOME, and Diethyl ether.

Property	Jet A-1	WCOME	DEE $(C_2H_5)_2O$
Specific gravity at 20 °C	0.797	0.877	0.715
kinematic viscosity at 40 °C (cSt)	1.08	3.14	0.23
Surface tension (N/m)	0.0265	0.0341	0.0148
Cetane number	46 ~ 48	51	120
Flashpoint (°C)	39	130	−40
Boiling point (°C) at 1 atm	163	350	34.6
Lower calorific value (MJ/kg)	43.46	39.98	36.84
Molecular weight (kg/kmol)	148.0	290.9	74.1
Elemental analysis (%) by mass:			
Carbon	86.51	77.22	64.90
Hydrogen	13.48	11.46	13.5
Sulfur	Nil	Nil	Nil
Oxygen	Nil	11.3	21.6
Nitrogen	Nil	Nil	Nil
H/C ratio	1.869	1.887	2.495

Table 5
Mixing ratios by vol. of the test fuels.

Fuel Abbreviation	Jet A-1	WCOME	DEE
Jet A-1	100%	–	–
B20	80%	20%	–
B20D10	70%	20%	10%
B20D30	50%	20%	30%

Table 6
Physical and chemical Main properties of the test fuels.

Property	Jet A-1	B20	B20D10	B20D30
Specific gravity at 20 °C	0.797	0.8137	0.8081	0.7918
kinematic viscosity at 40 °C (cSt)	1.08	1.20	1.185	0.971
Surface tension (N/m)	0.0265	0.0280	0.0267	0.0241
Flash Point (°C)	39	–	–	–
Lower calorific value (MJ/kg)	43.46	42.32	41.97	41.25
Molecular weight (kg/kmol)	148.0	176.6	169.2	154.4
Elemental analysis (%) by mass:				
Carbon	86.51	85.18	83.00	78.67
Hydrogen	13.48	13.29	13.30	13.30
Sulfur	Nil	Nil	Nil	Nil
Oxygen	Nil	1.516	3.693	8.020
Nitrogen	Nil	Nil	Nil	Nil
H/C ratio	1.87	1.88	1.92	2.03
Stoichiometric air/fuel ratio	14.53	14.25	13.90	13.23

samples fully evaporate at about 340℃, an air-preheated temperature of 350℃ was chosen to achieve more complete evaporation rather than partially pre-vaporized combustion to achieve LPP combustion conditions, which can be used in gas turbine applications.

2.3. Testing procedures and operating conditions

In order to perform the targeted experiments, the air accumulator tank is first drained of the condensed humidity, and the compressor is turned on after adjusting the startup and shutdown pressures. Then, the airflow rate is calculated via the rotameter and air pressure gauge readings and adjusted to get the desired quantity. Next, the air heaters are switched on and adapted to the desired temperature previously chosen from the TGA assessment of test fuels (typically 350 ± 2 ℃). After that, the fuel pump is switched on to supply the fuel into the system, followed by adjusting the fuel flow rate to obtain a constant equivalence ratio, typically 0.85. Finally, the premixed fuel/air mixture is sparked using the ignition electrodes to start combustion. When the wall thermocouple readings become steady, the local flame temperature and species concentration are measured at each predefined discrete point using the 2-D traverse mechanism.

During the experiments, the preheated air temperature was maintained at 350℃ to ensure the system component's safe operation. Also, the equivalence ratio was tuned to obtain a lean equivalence ratio that achieved a stable flame. This equivalence ratio (Φ) was selected to be 0.85 and kept constant during all experiments by tuning the fuel and air flow rates. The test conditions of the experiments are summarized in Table 7.

2.4. Measurement techniques

The measurements required for the current study include temperature (inside the flame at various locations throughout the combustion chamber and along the combustion chamber wall) and local species concentration.

2.4.1. Temperature measurements

A type R thermocouple (platinum/platinum-13% rhodium) with ceramic tube insulation was used for the temperature measurements. The thermocouple had a wire diameter of 100 μm and a bead diameter of 0.6 mm, and it was pre-calibrated, and the equation (1) was used to fit the calibration curve:

$$T_{corr(℃)} = 1.0008\ T_{meas(℃)} + 0.1225 \quad (1)$$

Where T_{corr} and T_{meas} are the corrected and measured temperatures in degree Celsius. All thermocouple signals were automatically recorded using a DAQ Card (Model NI USB-9213) and stored on a personal computer using the LabView software. The DAQ records the readings at a rate of 100 samples per second. The recorded data is then post-processed to obtain the average of the measured values. Due to the thermal radiation to the combustor wall, the flame thermocouple readings were corrected against this radiation heat loss according to the El-Zoheiry et al. approach [29]. This method briefly applies energy balance as expressed by equation (2):

$$h(T_{ac}\text{-}T_{meas}) = \varepsilon\sigma(T^4_{meas} - T^4_{sur}) \quad (2)$$

Where T_{ac}, T_{meas}, and T_{sur} are the actual, measured, and surrounding temperatures, ε is the thermocouple bead emissivity, s is the Stefan Boltzmann constant, and h is the convection heat transfer coefficient at the surface of the thermocouple bead. It was assumed that the thermocouple bead was a sphere with a diameter of 0.6 mm, and combustion was supposed to be complete. The Nusselt number (Nu) was determined from equation (3) for forced convection heat transfer around a sphere:

$$Nu = \frac{hD}{K} = 2 + \left[0.4Re^{\frac{1}{2}} + 0.06Re^{\frac{2}{3}}\right]Pr^{0.4}\left(\frac{\mu_\infty}{\mu_s}\right)^{\frac{1}{4}} \quad (3)$$

Where R_e is the Reynolds number, and P_r is the Prandtl number, and they are calculated from equations (4) and (5):

$$Re = \frac{\rho v D}{\mu_\infty} \quad (4)$$

$$P_r = \frac{\mu_\infty C_p}{K} \quad (5)$$

Where ρ is combustion product density, μ_∞ is combustion product viscosity, C_p is constant pressure specific heat, K is thermal conductivity, and μ_s is the mixture viscosity. μ_∞, K, C_p, and ρ are calculated at the adiabatic flame temperature (T_{ad}), while (μ_s) is calculated at the thermocouple temperature (T_{meas}) using Wilke's method [30].

A two-dimensional traverse mechanism was used to support the thermocouple rod to measure temperature through the flame zone at the predetermined sampling points, as shown in Fig. 5(a).

2.4.2. Species concentration measurement

The hot product gases were collected by using a water-cooled sampling probe (8 mm outside diameter) at the points shown in Fig. 5(b). The sampling probe was fitted with a multi-gas analyzer (ECOM-J2KN

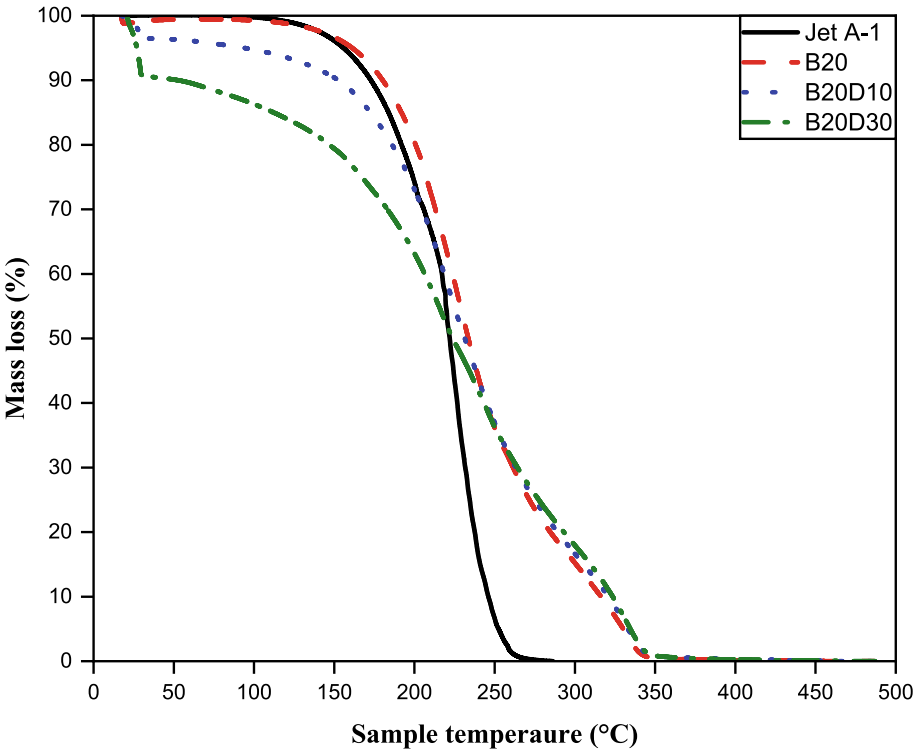

Fig. 4. TGA of the tested fuels.

Table 7
Experimental test conditions.

Case no.	Fuel	Fuel flow rate, kg/h	Air flow rate, kg/h	Air preheated temperature, ℃	Equivalence ratio, Φ
1	Jet A-1	1.23	21.04	350	0.85
2	B20	1.26			
3	B20D10	1.29			
4	B20D30	1.35			

Pro). Table 8 shows each cell type, measuring range, accuracy, and principle. Measuring the temperature and species concentration separately may be preferable to obtain more accurate readings because the sampling probe is 8 mm in diameter and water-cooled, so the effect of thermal radiation on the temperature measurement accuracy would be significant.

Uncertainty is the range of error values for a specific measurement. Kline [59] deduced that the uncertainty of a result R could be represented as in equation (6):

$$WR = \sqrt{\left(\frac{\partial R}{\partial x_1}W_{x_1}\right)^2 + \left(\frac{\partial R}{\partial x_2}W_{x_2}\right)^2 + \cdots + \left(\frac{\partial R}{\partial x_n}W_{x_n}\right)^2} \quad (6)$$

Where W is the uncertainty of the variable and x_1,x_2, and x_n are the measured values. The present work conducts an uncertainty analysis for flame temperature and species concentration measurements. The maximum uncertainty of flame temperature was 0.735%, and the maximum uncertainties of species concentration were equal to the resolution ratio to the measuring range, as shown in Table 8.

3. Results and discussion

The combustion and emission characteristics of the tested fuels are discussed in the following subsections.

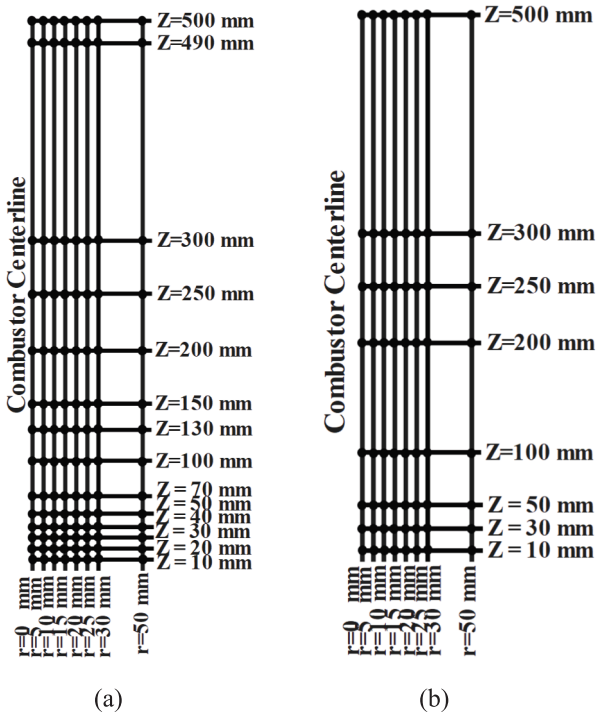

Fig. 5. Sampling points of (a) temperature and (b) species.

3.1. Combustion characteristics

In combustion research, the flame temperature is a significant characteristic that provides practical concepts for investigating combustion characteristics and emitted pollutants. Temperature contours for the investigated fuels are provided in Fig. 6 to give an overview of the

Table 8
Range and resolution of gas analyzer [31].

Parameter	Measuring range	Resolution	Maximum uncertainty	Principle
CO	0 ~ 6.3 vol%	0.01 vol%	0.16%	Infrared
CO_2	0 ~ 20 vol%	0.1 vol%	0.5 %	Infrared
NO	0 ~ 5000 ppm	1 ppm	0.02%	Electrochemistry
NO_2	0 ~ 1000 ppm	1 ppm	0.1%	Electrochemistry
O_2	21 vol%	0.1 vol%	0.48%	Electrochemistry

flame. It is found that the B20 blend has a higher flame temperature than Jet A-1 and other mixtures up to 70 mm above the burner, followed by the B20D10 combination (which also has a slightly higher temperature than Jet A-1), while the B20D30 mixture has a lower temperature than Jet A-1. Additionally, it is noticed that biodiesel and DEE significantly affected the flame shape, as biodiesel increases the flame width while DEE reduces the flame width, as seen in Fig. 6.

To describe the flame in more detail, the flame temperature is plotted versus the radial location at different levels throughout the combustor, as shown in Fig. 7. At all radial locations, the flame temperatures are low at the bottom, where initiation reactions are still in progress and accelerate rapidly as the reactions are affected by the chemical (for premixed mixtures) and physical (for the swirled flow) flow characteristics. The initiating and branching reactions also dominate this region, so the flame temperature continues to rise until it reaches its maximum value within the recirculation zone formed by the swirling flow. After that, all product reactions become dominant, so products begin to freeze. For example, the maximum flame temperature for the Jet A-1 is 2074 K, while the maximum flame temperatures for the B20, B20D10, and B20D30 blends are 2061, 2079, and 2092 K, respectively, and they were all recorded at Z = 40 mm. The flame temperature is mainly affected by the heating value, H/C ratio, oxygen content, viscosity, and degree of atomization and evaporation achieved by fuel molecules prior to entering the flame zone.

Fig. 7 shows that the B20 blend has a higher flame temperature than other blends up to 70 mm above the burner, although biodiesel has a lower calorific value than Jet A-1. After that, it starts to decrease gradually. It could be due to the poor atomization of biodiesel, which creates fuel droplets that do not have sufficient time and energy to evaporate fully before entering the flame zone. These droplets mix with the incoming air inside the combustor, which causes partial diffusion combustion at the stoichiometric condition ($\Phi = 1$) at the surface, and the flame temperature reaches its maximum value compared with the lean condition combustion ($\Phi < 1$) of Jet A-1. Also, these droplets created by poor atomization are relatively heavier, and the inertia of the incoming air cannot lift them axially through the combustor, while the swirler creates angular momentum. Therefore, they escape radially towards the wall to burn far from the burner centerline and cause hot spots in the combustor. At higher levels, the WCOME droplets gradually evaporate, and the heterogenous mixture disappears; the mixture gains more homogeneity, and the flame temperature distribution becomes closer to the Jet A-1, as shown in Fig. 7. Another explanation can be attributed to the existence of more double bonds in WCOME that raise the adiabatic flame temperature and, thus, increase the flame temperature [32,33]. This observation is confirmed by the results reported by Kumar et al. [34].

With the addition of 10% DEE, the flame temperature of the B20D10 blend slightly decreases, but it is still higher than Jet A-1. This temperature reduction indicates better atomization, a smaller SMD, an enhanced evaporation rate, and adequate mixing between fuel and air, finally resulting in a homogenous mixture. This is because the addition of DEE reduces the fuel viscosity as well as surface tension and improves the atomization process, leading to an enhancement in the fuel evaporation rate and the mixing intensity with air. This also contributes to more complete evaporation of the fuel, resulting in more homogeneity of the fuel–air mixture, and the fuel combusts with a premixed combustion mode in the combustor compared with the partial diffusion combustion mode of unevaporated fuel droplets for the B20 blend, and this is

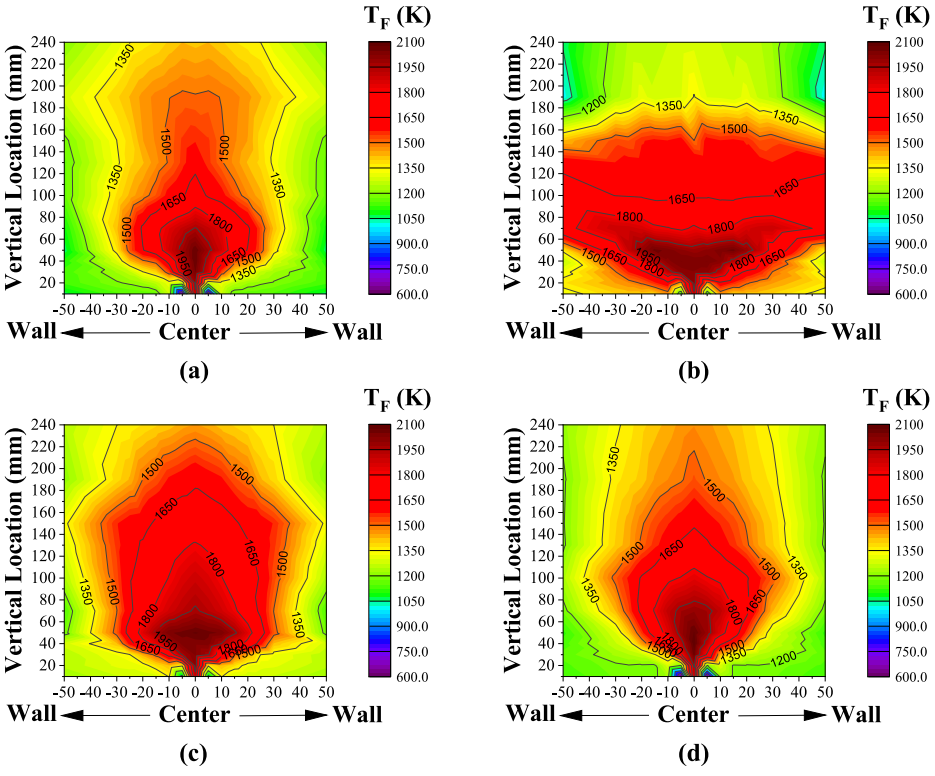

Fig. 6. Contours plot of the flame temperature of (a) Jet A-1, (b) B20, (c) B20D10, and (d) B20D30 throughout the combustor.

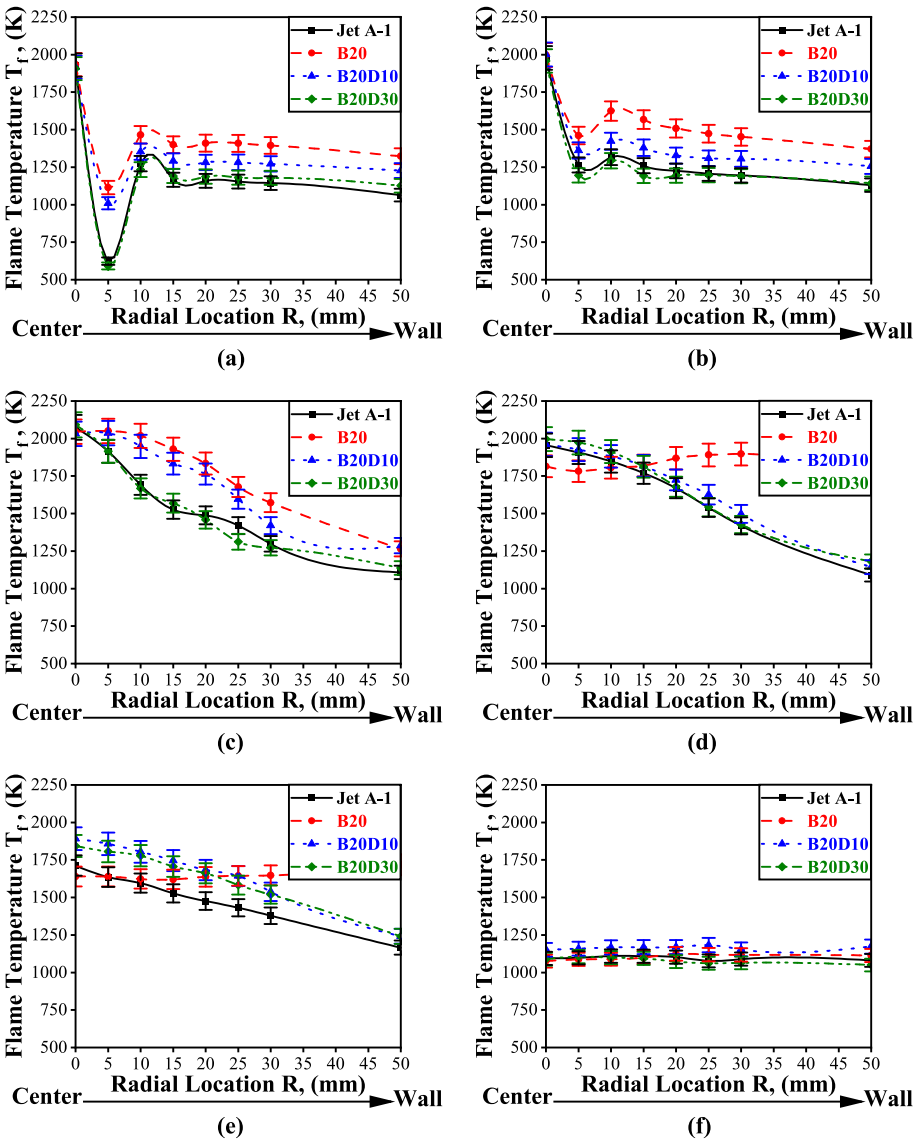

Fig. 7. Radial flame temperature distribution of the test fuels throughout the combustor at (a) Z = 10, (b) Z = 20, (c) Z = 40, (d) Z = 70, (e) Z = 100, and (f) Z = 500 mm.

obvious in Fig. 7 [35].

At 30% DEE addition, the flame temperature decreases up to 70 mm above the burner, is followed by an increase relatively beyond this level, and again returns to declining from 240 mm above the burner until it reaches the combustor exit. This may also be due to the higher oxygen content in the fuel, which increases the oxidation rate of fuel enhanced combustion efficiency [36]. However, despite the increase in oxygen level in the fuel blend that can improve the fuel oxidation rate and combustion efficiency, it may cause a dilution of the mixture, thereby reducing the flame temperature [36]. While the significant fluctuation in flame temperature may be due to the higher volatility of DEE, which induces vapor bubbles and vapor lock in the fuel nozzle when DEE is employed in a more significant proportion in the fuel blend [37], this problem can be avoided by cooling the nozzle.

DEE blends have better atomization because DEE's surface tension is about 0.0148 N/m compared with 0.0341 N/m for WCOME and 0.0265 N/m for Jet A-1. Also, DEE has a lower viscosity than WCOME and Jet A-1 (typically, it is 0.23 cSt compared with 3.14 and 1.08 cSt for WCOME and Jet A-1, respectively). Therefore, the best parameter to describe the degree of atomization is Sauter Mean Diameter (SMD), which can be calculated for test fuel according to the empirical equation (7) by Lefebvre and Ballal [38]:

$$SMD = 2.25\sigma^{0.25}\mu_l^{0.25}\rho_a^{-0.25}\Delta P_l^{-0.5}m^{0.25} \quad (7) \tag{7}$$

Fig. 8 shows the SMD of the tested fuels. It is observed that the B20 blend has the largest SMD (typically 8.64 μm), while the B20D30 combination has the smallest SMD (normally 7.83 μm). Adding 20% WCO biodiesel to Jet A-1 increases the droplet SMD by 7.2%, while adding 30% DEE to the B20 blend reduces the droplet SMD by 9.38% relative to the B20 blend. On the other hand, the SMD of the B20D30 blend is very close to Jet A-1. This means that adding WCO biodiesel to Jet A-1 increases the size of droplets, while adding DEE to the biodiesel/Jet A-1 blend reduces them.

A significant parameter that must be considered in gas turbine combustion is the pattern factor (PF), which describes the thermal uniformity throughout the combustion chamber [39]. The pattern factor (PF) is calculated for all tested fuels at different levels. The smaller the pattern factor, the better the combustor's thermal uniformity [39]. PF is a dimensionless parameter that can be calculated using equation (8):

$$PF = \frac{T_{max} - T_{min}}{T_{mean} - T_{in}} \tag{8}$$

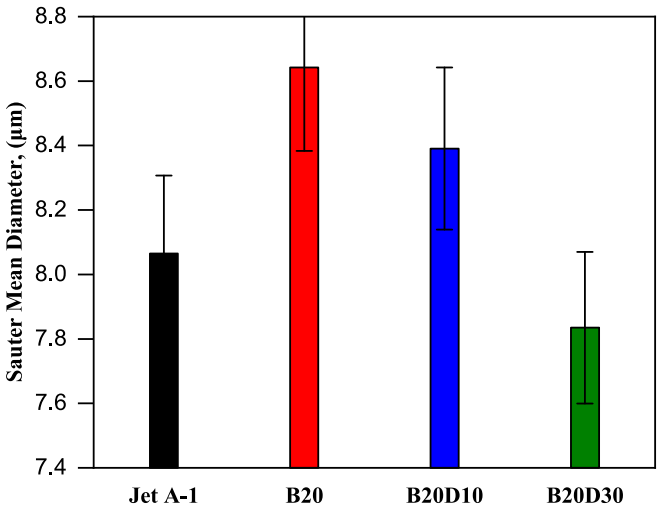

Fig. 8. Sauter Mean Diameter of the test fuels.

Where T_{max} is the maximum recorded temperature, T_{mean} is the mean exit temperature, and T_{in} is the inlet air temperature. As shown in Fig. 9, for all the test fuels, the pattern factor profile begins with a considerable value and then decreases gradually until the end of the combustion chamber. It is also observed that the lowest value of pattern factor among other test fuels is the B20 blend. This is a result of the WCOME droplets undergoing combustion in the lower zone of the combustor.

It is also observed in Fig. 9 that adding DEE leads to an increased effect on the pattern factor. This is because DEE plays an essential role in enhancing fuel atomization and reducing the chance of combustion droplet occurrence, so the flame temperature decreases, especially near the combustor wall, due to the lower heating value of the fuel.

3.2. Emission characteristics

Emission characteristics of swirling lean prevaporized premixed (LPP) combustion are mainly dominated by certain factors such as fuel type, flow field, turbulence intensity, equivalence ratio, inlet temperature, local flame temperature, residence time, and mean spray droplet size [35]. Therefore, the current study investigated the impacts of different fuel types by keeping the other test conditions constant, as previously provided in Table 7. In addition, the recorded measurements are normalized to the reference condition of 15% oxygen on a dry basis to avoid the effect of air dilution and to compare experimental data without ambiguity.

Carbon monoxide (CO) is an intermediate species produced during carbon oxidation to carbon dioxide (CO_2). Furthermore, CO can be formed by the dissociation of CO_2 in locations where the flame temperature exceeds 1800 K. Thus, the generation of CO at low temperatures is primarily the result of incomplete combustion, while at high temperatures, it is mainly dominated by CO_2 dissociation processes. Fig. 10 shows the radial distribution of CO concentration inside the flame. Thus, only the best levels illustrating the CO concentration throughout the combustor are presented. In all test fuels, the CO concentration increases and then gradually decreases along the axial combustor, and the flame temperatures are low. Also, as the radial distance from the centerline of the burner increases, CO concentrations decrease, reaching a minimum at the farthest point near the combustor wall. It is also noticed that, up to Z = 100 mm, CO distribution fluctuates arbitrarily due to the effect of the swirler recirculation zone. CO concentrations are higher at these lower levels due to the activity of free radicals and the oxygen richness in the primary reaction zone. In addition, the high temperatures in this reaction zone help in promoting CO_2 dissociation. Beyond Z = 100 mm, CO concentrations show a decline with relatively homogenous patterns up to the combustor exit with an average value of 15 ppm. This is because the free radicals responsible for CO production consuming to complete the combustion reaction of the lean premixed mixture, and the mixture becomes more homogeneous. This behavior was also observed by Johnson et al. [40].

By the comparison beyond Z = 100 mm and up to the combustor exit, Jet A-1 records the highest concentration of CO, while the CO concentration of the B20D30 blend is the lowest. The reduction trend is continued for the B20D10 and B20 blends compared with Jet A-1, where it is 68, 15.8, and 7.6%, respectively, at the combustor exit. This decrease in the CO concentration of the B20 blend is mainly caused by

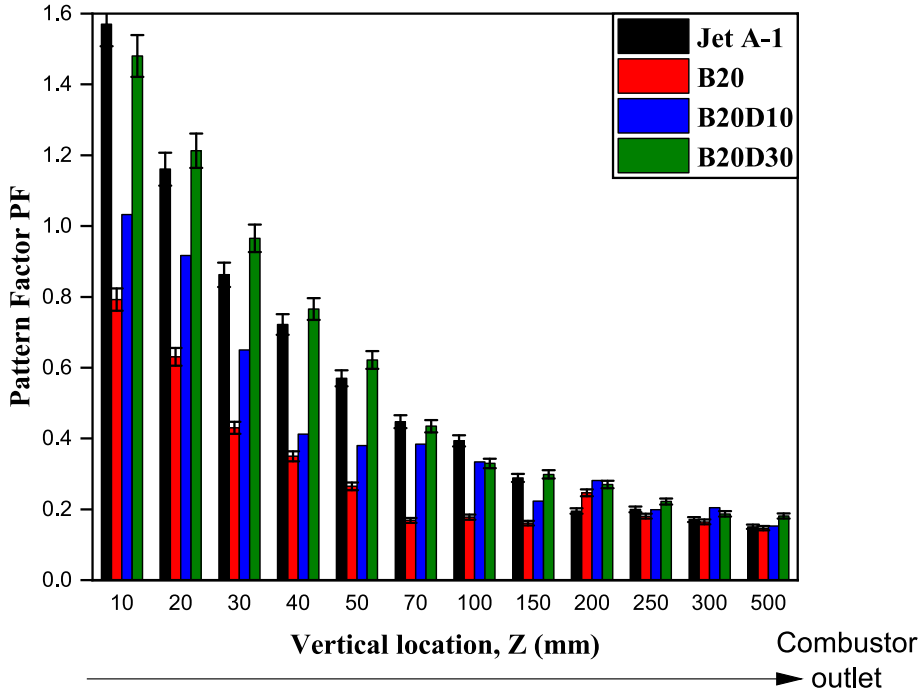

Fig. 9. Combustor pattern factor of the test fuels.

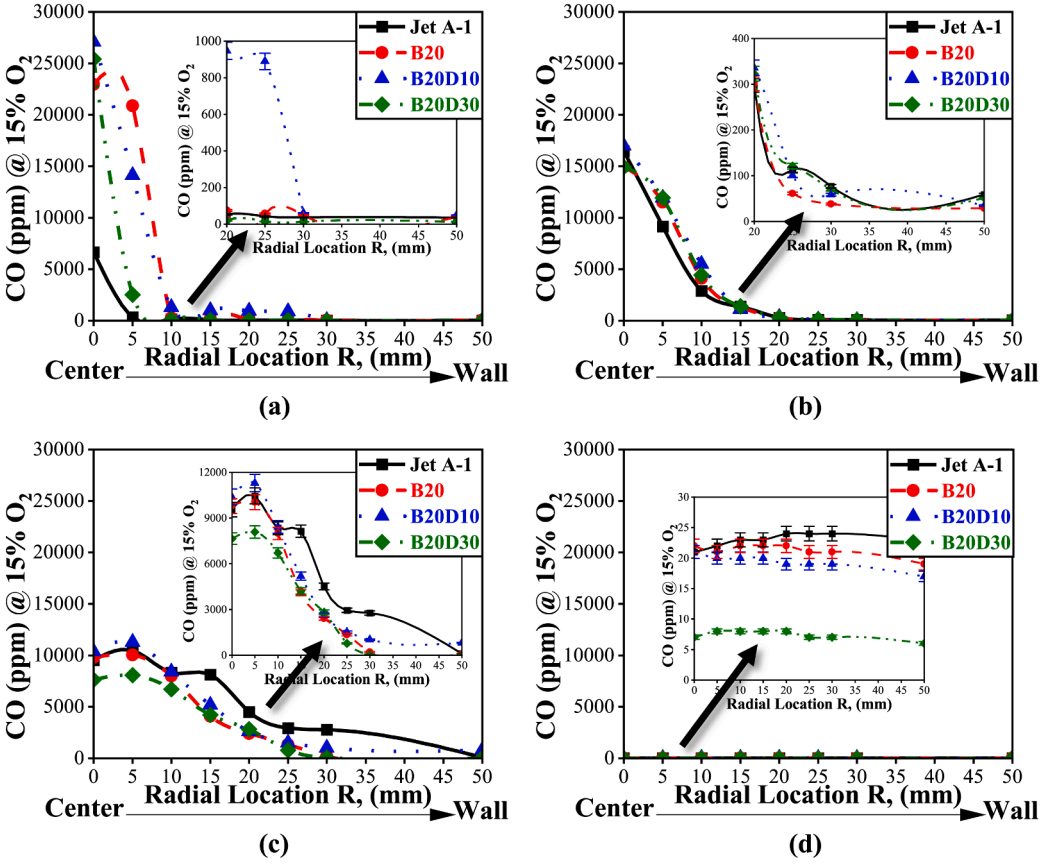

Fig. 10. Radial distribution of CO concentration throughout the combustor at (a) Z = 10, (b) Z = 30, (c) Z = 50, and (d) Z = 500 mm.

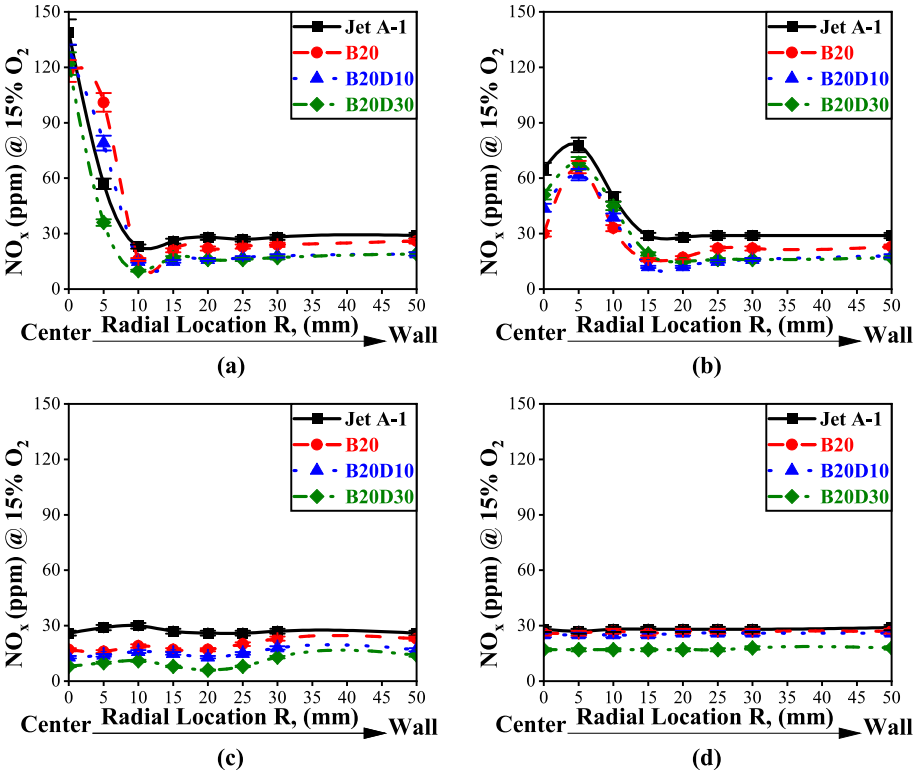

Fig. 11. Radial distribution of NOx concentration throughout the combustor at (a) Z = 10, (b) Z = 30, (c) Z = 50, and (d) Z = 500 mm.

biodiesel's oxygen content, which promotes fuel oxidation and aids in the oxidation of CO into CO_2, resulting in a lower CO concentration [32]. This observation was confirmed with similar results by Habib et al. [4]. Also, the decrease in CO concentration of the DEE blends could be due to much more oxygen molecules (which makes a dilution for the mixture resulting in reduced temperature), a higher cetane number in DEE, and the proper mixing of fuel and air with enhanced spray atomization, resulting in much reduction in the CO emissions [1,13].

The nitrogen oxides (NO_x) formation mechanisms in lean premixed combustion are primary prompt and thermal NO_x. The prompt NO_x is created when hydrocarbon fragments react with nitrogen to form nitrogen species like HCN [41], while the thermal NO_x (Zeldovich) mechanism is an endothermic reaction generating NO at high temperatures of around 1,850 K [39]. Several factors contribute to the formation of thermal NO_x, including the local and adiabatic flame temperatures, the degree of turbulence, flue gas residence time, oxygen content, spray characteristics, and the local equivalence ratio inside the flame [39 42]. Like the CO trend, Fig. 11 shows the variation of NO_x throughout the combustor. It can be noticed that NO_x begins with an increase in lower levels due to the high temperatures, which promote the thermal NO_x, then gradually decreases with the vertical distance, reaching a minimum value at the combustor exit.

Furthermore, it also shows that the B20D30 blend has the lowest NO_x concentration, followed by the B20D10 and the B20 combinations, while Jet A-1 has the highest NO_x level. The reductions are 38.4, 8.9, and 4.9%, respectively, compared with Jet A-1 at the combustor exit. The reason could be attributed to the lower tendency to prompt the NO_x mechanism [41]. Prompt NO_x is proportional to the carbon content of the fuel [43]. Biodiesel has a lower carbon content than Jet A-1 by 10.7%, as presented in Table 4. This means that it has a lower tendency to form prompt NO_x. Also, the main reason could be attributed to DEE having a high cetane number, which shortens the ignition delay and the mixing formation time, reducing the peak temperature [42]. Additionally, the high latent heat of DEE vaporization helps lower combustion temperatures, decreasing thermal NO_x emissions [42]. Furthermore, DEE has a lower carbon content than Jet A-1 by 25% compared with 10.7% for biodiesel, as listed in Table 4, which reduces the tendency for prompt NO_x formation.

Unburned hydrocarbons (UHC) refer to the unburned fuel that escapes from the combustor as droplets or vapor, in addition to the smaller molecular weight products resulting from the thermal degradation of the fuel [39]. UHC is dominated by several factors like fuel properties, poor atomization, low burning rate, homogeneous or heterogeneous mixture combustion, and quenching of the combustion products [39]. The UHC emissions of the test fuels are illustrated in Fig. 12. Like the NO_x and CO trend, UHC fluctuates arbitrarily, attributing to the effect of the swirler recirculation zone. There is a decrease in UHC emissions for the B20D30, B20D10, and B20 blends of about 43.4, 51.4, and 35.3%, respectively, at the combustor exit. This may be attributed to the high oxygen content of DEE needed to initiate the unsaturated hydrocarbons in the fuel, which causes more complete and cleaner combustion [44]. However, the decrease is only 43.4% for the B20D30 blend, compared with 51.4% for the B20D10 blend. This is due to DEE including a high latent vaporization heat, causing a reduction in the combustion temperature, especially near the combustor wall during the mixture formation [1]. In this case, the UHC level is higher for the B20D10 blend than for Jet A-1 at the combustor boundary. It is also due to the high volatility of DEE, which causes easier evaporation of its excess, leaving behind a mixture zone with a lower concentration of DEE and less oxygen.

Many factors directly impact carbon dioxide (CO_2) emissions, like the H/C ratio, blend density, incomplete combustion, and the total oxygen content of the fuel [45]. Fig. 13 shows the CO_2 emissions of the test fuels throughout the combustor. Unlike CO behavior, CO_2 begins with a low concentration at the burner's center line of low levels, where the activity of free radicals and the high flame temperature promote CO_2 dissociation, as previously discussed in Fig. 10. Then it gradually increases with the vertical distance, where the flame temperature decreases, and the CO is oxidized to CO_2. There is a decrease in CO_2 emissions for the B20D10 and B20D30 blends of 6.17 and 14.5% relative to Jet A-1, respectively, at the combustor exit. While the B20 blend recorded an increase in CO_2 emissions of 5.33%. This may be attributed to the complete combustion achieved by blending DEE with biodiesel,

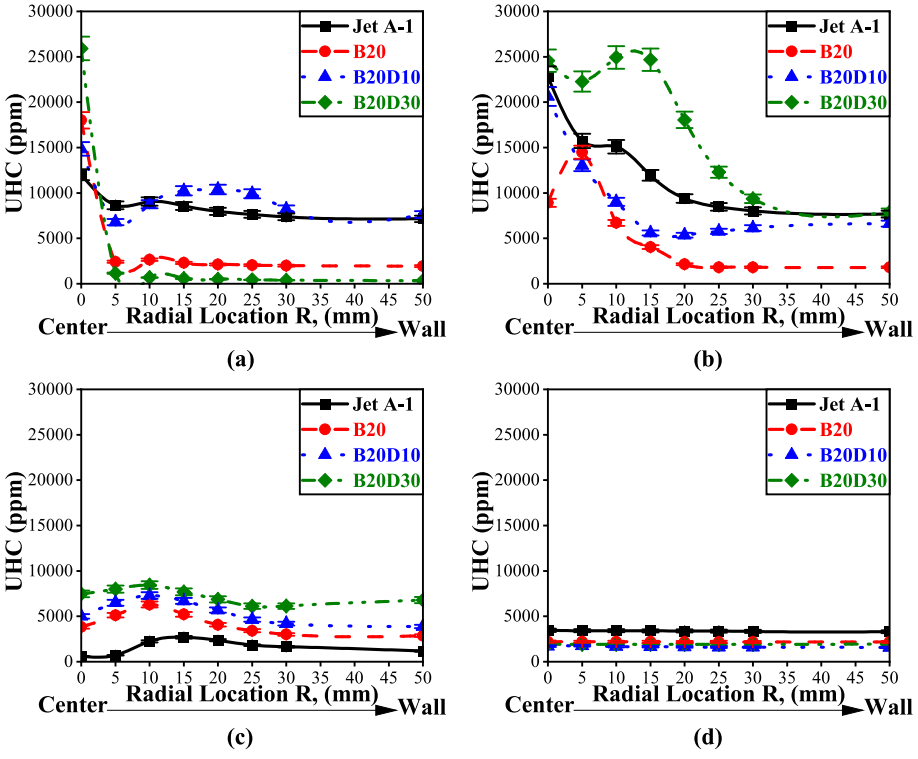

Fig. 12. Radial distribution of UHC concentration inside the flame at (a) Z = 10, (b) Z = 30, (c) Z = 50, and (d) Z = 500 mm.

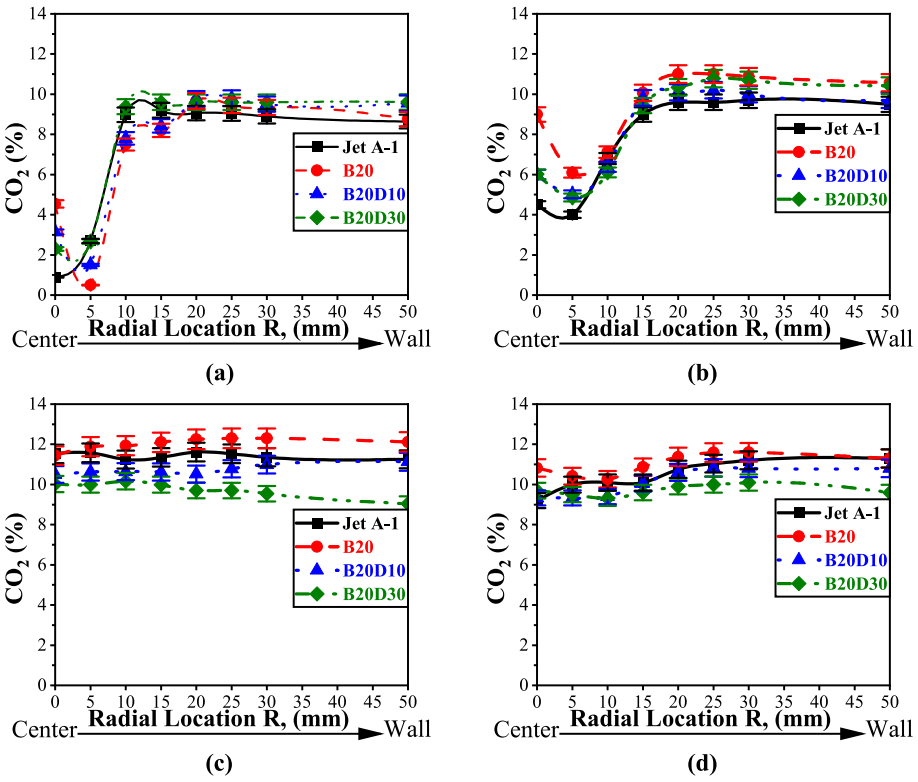

Fig. 13. Radial distribution of CO_2 percentage inside the flame at (a) Z = 10, (b) Z = 30, (c) Z = 50, and (d) Z = 500 mm.

improving combustion characteristics [46]. Carbon neutrality is the main significant advantage of biodiesel since plants reabsorb CO_2 released during combustion during their growth. As a result, there should be no net increase in carbon emissions [47]. On the other hand, the net result is not zero carbon emissions [47]. Because the energy requirements for biodiesel production result in CO_2 emissions [47].

To investigate the environmental impact of Jet A-1 fuel blended with WCOME and DEE, the average emission indices for both NO and CO (EI_{NOx} and EI_{CO}) at the combustor exit were calculated and presented in Fig. 14 in (mg/MJ of fuel) to overcome the heating value differences of the test fuels according to equation (9) by Turns [48]:

$$\mathbf{EI}i = \left(\frac{\chi_i}{\chi_{CO} + \chi_{CO_2}}\right)\left(\frac{x_c \mathbf{MW_i}}{\mathbf{MW_f}}\right) \Big/ \mathbf{LHV}_f \tag{9}$$

As shown in Fig. 14, the B20D30 blend achieved the lowest CO and NO_x emission index, while Jet A-1 achieved the highest emission index for both CO and NO_x, with a reduction of 65% and 32.6% relative to Jet A-1, respectively. This could be due to much more oxygen molecules, a higher cetane number in DEE, the proper mixing of fuel and air with enhanced spray atomization, and a lower flame temperature resulting in much reduced CO and thermal NO_x emissions [1,13]. This also means that it has a lower tendency to form prompt NO_x where the flame temperature is low. It is also noticed that EI_{NOx} and EI_{CO} for the B10D10 blend are slightly higher than those of the B20 mixture, despite emitting lower concentrations of CO and NO_x than the B20 blend. This is because the B20D10 blend has a lower molecular weight and LHV than the B20 blend, and the CO and NO_x reduction of the B20D10 blend relative to the B20 mixture is small.

4. Comparison with previous studies

Table 9 lists the recent studies and their findings when applying

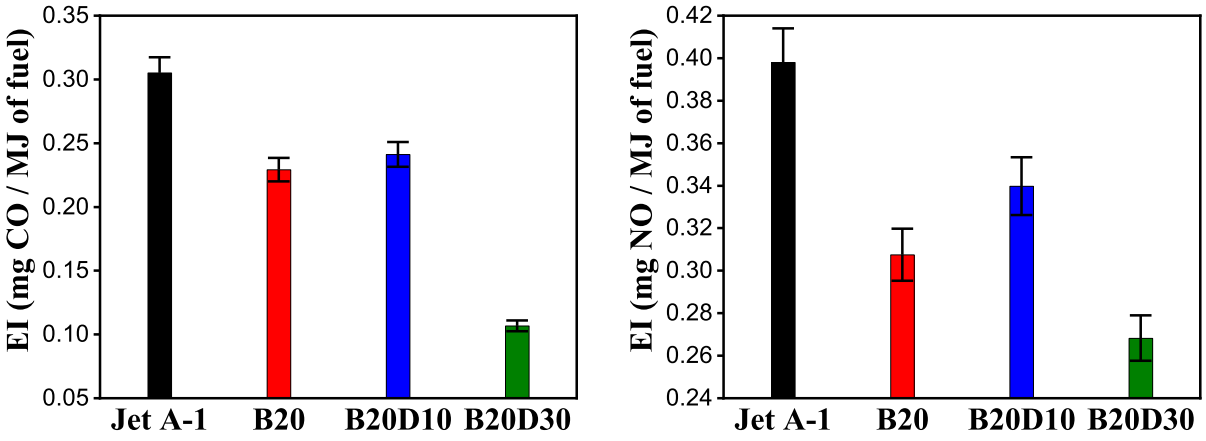

Fig. 14. Average EI_{CO} and EI_{NOx} of the test fuel at the combustor exit.

biodiesel in LLP combustors or adding ether fuels to biodiesel. Masoud et al. [26] investigated the effects of WCOME blended with jet A-1 at a single blending ratio of 10% WCOME on flame and emission characteristics in an LLP combustor, and they found that biodiesel achieved lower NO_x levels, comparable flame temperature distribution with jet A-1, and good thermal homogeneity throughout the combustor, but higher CO levels were observed. Also, Attia et al. [35] studied the effects of WCOME-jet A-1 blends at four mixing ratios of 5, 10, 15, and 20%. They found a decrease in flame temperature and exhaust emissions of 70% for CO concentration and 58% for NO_x levels for the B20 blend.

In addition, El-Zoheiry et al. [41] and Kumar et al. [34] found a reduction in CO, NO_x, and UHC in JOME and Limonene blends, respectively. Finally, Zhan et al. [14] examined the addition of ethanol and DEE to soybean biodiesel-diesel blends in a constant-volume combustion chamber. They revealed that biodiesel increases droplet size. Also, ethanol or DEE addition to diesel–biodiesel blends decreased the droplet size, enhancing the atomization process of diesel–biodiesel blends. Thus, when comparing the current results with previous findings, many enhancements in physical, chemical, and combustion characteristics with DEE addition were recorded. DEE additives also played the primary role in reducing pollutant emissions, which reached a decrease of 68% in CO emissions, 38.4% in NO_x emissions, and 51.4% in UHC emissions, but the flame temperature is comparable.

5. Conclusions and recommendations

In the present investigation, DEE is added to a biodiesel-Jet A-1 blend with different blending ratios to study the effect of adding DEE on combustion characteristics in a swirl-stabilized LPP combustor and compare it with Jet A-1. The tests are performed by burning Jet A-1, B20, B20D10, and B20D30 blends in the LPP combustor while keeping all operating conditions constant, like the preheated temperature (350 ℃) and equivalence ratio ($\Phi = 0.85$). In addition, the local temperature and species concentration distributions inside the combustor are analyzed. The following findings have been concluded from the data analyses:

1. DEE addition enhanced biodiesel physicochemical properties like viscosity by 19.1%, surface tension by 14.1%, and SMD by 9.38% with 30% DEE addition relative to the B20 blend.
2. The flame temperature distributions of DEE blends were comparable to Jet A-1, while the B20 blend showed a variation compared with Jet A-1.
3. Jet A-1 achieved the maximum flame temperature (2,074 K), while the B20 blend achieved the lowest (2,061 K). On the other hand, the B20 mixture exhibited the lowest pattern factor (0.146) compared with Jet A-1 (0.151) at the combustor exit, indicating a more uniform temperature distribution throughout the combustor by 3.3% than Jet A-1.
4. CO levels were lower for the B20D30 blend than Jet A-1 by 68% at the combustor exit, with an average value of 7 and 23 ppm, respectively.
5. The B20D30 blend resulted in the lowest NO_x levels, with an average value of 17 ppm compared with an average value of 28 ppm for Jet A-1 at the combustor exit; the decrease was 38.4% relative to Jet A-1.
6. CO_2 emissions were reduced by 14.5% compared with Jet A-1 at the combustor exit, with a 30% DEE addition.
7. UHC level decreased with 10% DEE by 51.4% compared with Jet A-1, while it decreased by 43.4% with adding 30% DEE.

Table 9
Previous studies of applying biodiesel in LLP combustors and adding ether fuels to biodiesel.

Ref.	Base Fuel	Additive Category	Blending ratio	Experimental configuration	Test Conditions	Results
[26]	Jet A-1	WCOME	• B0 • B10	Swirl stabilized LPP combustor	• SN = 0.55 (Radial swirler) • T_a = 310 ℃ • Φ = 0.75	• Higher CO but lower NO_x levels for the B10 blend. • Higher thermal homogeneity of combustor for B10 blend. • Comparable flame temperature distribution for both fuels.
[35]	Jet A-1	WCOME	• B0 • B5 • B10 • B15 • B20	Swirl stabilized LPP combustor	• SN = 0.55 (axial swirler) • T_a = 250 ℃ • Φ = 0.75	• Decreased flame temperature and exhaust emission by 70% for CO and 58% for No_x for the B20 blend. • Similar flame temperature distribution with base fuel (Jet A-1).
[41]	Jet A-1	JOME	• B0 • B10 • B20	Swirl stabilized LPP combustor	• SN = 0.78 (axial swirler) • T_a = 250 ℃ • Φ = 0.87 & 0.95	• Reduced local flame temperature and a slight reduction in CO, NO_x, and UHC in JOME blends
[34]	Jet A-1	Limonene	• B0 • B10 • B30 • B50	Axial swirl stabilized spray combustor	• SN = 0.78 (axial swirler) • T_a = 100 ℃ & 200 ℃ • Φ = 0.50	• CO decreased by 15% for the B50 blend. • Higher temperature profile of limonene blends than jet A-1.
[21]	Methyl decanoate (MD)	Dibutyl ether (DBE)	• MD100 • DBE10 • DBE20 • DBE30 • DBE40	Co-flow diffusion flame	• T_{fuel} = 573 K • T_{air} = 473 K	• DBE decreases soot formation.
[14]	Diesel (D)	Soybean biodiesel (B), ethanol (E), diethyl ether (DEE)	• D100 • B20 • B16E20 • B16DEE20	Spray combustion	• P_{inj} = 50, 100, 150, and 200 (MPa) • T_{fuel} = 25 ℃ • P_{amb} = 2 and 4 (MPa)	• Biodiesel increased SMD. • DEE decreased SMD. • DEE improved fuel atomization.
Current study	Jet A-1	WCOME and DEE	• Pure jet A-1 • B20 • B20D10 • B20D30	Swirl stabilized LPP combustor	• SN = 0.55 (Radial swirler) • T_a = 350 ℃ • Φ = 0.85	• Enhanced viscosity and SMD by 19.1% and 9.38%, respectively. • NO_x, CO, CO2, and UHC decreased by 38.4, 68, 14.5, and 43.4%, respectively.

8. Overall, the B20D30 blend was better regarding NO_x and CO levels, while the B20D10 mixture was better regarding the flame temperature profile and UHC levels.

The above findings support replacing Jet A-1 with the B20D30 blend in gas turbines without causing issues or requiring modifications to the combustor design.

The empirical findings presented here must be evaluated in light of certain limitations. The first limitation was that using compressed air without an air dryer unit has an effect on results as the water vapor included in the air plays a role in the combustion process, such as decreasing the combustion temperature, and hence affects various parameters like CO, NO_x, CO_2, and UHC concentrations. The second limitation was that the thermal heat radiation loss to the combustor wall is significantly affected by the bead diameter of the thermocouple and needs to be corrected against this loss. Therefore, using a thermocouple with a finer bead diameter would effectively solve this issue. But the high price and periodic cracking of the junction prohibited using it. The third limitation was the limited power of the air heaters, which did not permit using fuels with a higher boiling point. Therefore, it is essential to suggest the following tips as recommendations for future work:

1. Supply the compressor with an air dryer unit to dry the humid air before using it for combustion.
2. Using a finer bead diameter thermocouple to measure the flame temperature with minimum thermal radiation loss and increase the accuracy of the measurement process.
3. Increasing the power capacity of air heaters to allow for using high-latent heat fuels.
4. If using higher blending ratios of DEE, adding energetic nanoparticles as additives could be a good solution to compensate for the decrease in the calorific values of blends.
5. Extend the study parameters to consider emergy, life cycle analysis, and exergy.

CRediT authorship contribution statement

Radwan M. EL-Zohairy: Conceptualization, Formal analysis, Investigation, Writing – original draft, Writing – review & editing. **Ahmed S. Attia:** Formal analysis, Investigation, Writing – original draft, Writing – review & editing. **A.S. Huzayyin:** Conceptualization, Investigation, Formal analysis, Writing – review & editing. **Ahmed I. EL-Seesy:** Conceptualization, Formal analysis, Investigation, Writing – original draft, Writing – review & editing.

Declaration of Competing Interest

The authors declare that they have no known competing financial interests or personal relationships that could have appeared to influence the work reported in this paper.

Data availability

Data will be made available on request.

References

[1] Sivalakshmi S, Balusamy T. Effect of biodiesel and its blends with diethyl ether on the combustion, performance and emissions from a diesel engine. Fuel 2013;106:106–10. https://doi.org/10.1016/j.fuel.2012.12.033.

[2] Kumar M, Karmakar S. Combustion characteristics of butanol, butyl butyrate, and Jet A-1 in a swirl-stabilized combustor. Fuel 2020;281:118743. https://doi.org/10.1016/j.fuel.2020.118743.

[3] Lin L, Cunshan Z, Vittayapadung S, Xiangqian S, Mingdong D. Opportunities and challenges for biodiesel fuel. Appl Energy 2011;88:1020–31. https://doi.org/10.1016/j.apenergy.2010.09.029.

[4] Habib Z, Parthasarathy R, Gollahalli S. Performance and emission characteristics of biofuel in a small-scale gas turbine engine. Appl Energy 2010;87:1701–9. https://doi.org/10.1016/j.apenergy.2009.10.024.

[5] Sandouqa A, Al-Hamamre Z. Energy analysis of biodiesel production from jojoba seed oil. Renew Energy 2019;130:831–42. https://doi.org/10.1016/j.renene.2018.07.015.

[6] Aghbashlo M, Hosseinzadeh-Bandbafha H, Shahbeik H, Tabatabaei M. The role of sustainability assessment tools in realizing bioenergy and bioproduct systems. Biofuel Res J 2022;9:1697–706. https://doi.org/10.18331/BRJ2022.9.3.5.

[7] Balat M. Production of biodiesel from vegetable oils: a survey. Energy Sources, Part A Recover Util Environ Eff 2007;29:895–913. https://doi.org/10.1080/00908310500283359.

[8] Esfandabadi ZS, Ranjbari M, Scagnelli SD. The imbalance of food and biofuel markets amid Ukraine-Russia crisis: a systems thinking perspective. Biofuel Res J 2022;9(1640–7). https://doi.org/10.18331/BRJ2022.9.2.5.

[9] Foo WH, Koay SSN, Chia SR, Chia WY, Tang DYY, Nomanbhay S, et al. Recent advances in the conversion of waste cooking oil into value-added products: a review. Fuel 2022;324:124539. https://doi.org/10.1016/j.fuel.2022.124539.

[10] Mohamed M, Sherif N, Aboelazayem O, Elazab HA, Gadalla M, Saha B. Waste cooking oil management in Egypt: production of biodiesel-development of rapid test method. J Phys Conf Ser 2022;2305:012035. https://doi.org/10.1088/1742-6596/2305/1/012035.

[11] Hosseinzadeh-Bandbafha H, Nizami AS, Kalogirou SA, Gupta VK, Park YK, Fallahi A, et al. Environmental life cycle assessment of biodiesel production from waste cooking oil: a systematic review. Renew Sustain Energy Rev 2022;161:112411. https://doi.org/10.1016/j.rser.2022.112411.

[12] Li H, Altaher M, Andrews GE. Evaluation of combustion and emissions using biodiesel and blends with kerosene in a low nox gas turbine combustor. Proc ASME Turbo Expo 2010;1:545–53. https://doi.org/10.1115/GT2010-22182.

[13] Qi DH, Chen H, Geng LM, Bian YZ. Effect of diethyl ether and ethanol additives on the combustion and emission characteristics of biodiesel-diesel blended fuel engine. Renew Energy 2011;36:1252–8. https://doi.org/10.1016/j.renene.2010.09.021.

[14] Zhan C, Feng Z, Ma W, Zhang M, Tang C, Huang Z. Experimental investigation on effect of ethanol and di-ethyl ether addition on the spray characteristics of diesel/biodiesel blends under high injection pressure. Fuel 2018;218:1–11. https://doi.org/10.1016/j.fuel.2017.12.038.

[15] Agarwal AK, Chaudhury VH. Spray characteristics of biodiesel/blends in a high pressure constant volume spray chamber. Exp Therm Fluid Sci 2012;42:212–8. https://doi.org/10.1016/j.expthermflusci.2012.05.006.

[16] Wang X, Huang Z, Kuti OA, Zhang W, Nishida K. Experimental and analytical study on biodiesel and diesel spray characteristics under ultra-high injection pressure. Int J Heat Fluid Flow 2010;31:659–66. https://doi.org/10.1016/j.ijheatfluidflow.2010.03.006.

[17] Sarin A, Arora R, Singh NP, Sarin R, Malhotra RK, Kundu K. Effect of blends of Palm-Jatropha-Pongamia biodiesels on cloud point and pour point. Energy 2009;34:2016–21. https://doi.org/10.1016/j.energy.2009.08.017.

[18] Fu W, Li F, Meng K, Liu Y, Lin Q. Experimental and analysis of macroscopic spray characteristics of biodiesel blended with Di-n-butyl ether under inert conditions. Waste Biomass Valoriz 2020;11:3501–11. https://doi.org/10.1007/s12649-019-00689-8.

[19] Tran LS, Pieper J, Zeng M, Li Y, Zhang X, Li W, et al. Influence of the biofuel isomers diethyl ether and n-butanol on flame structure and pollutant formation in premixed n-butane flames. Combust Flame 2017;175:47–59. https://doi.org/10.1016/j.combustflame.2016.06.031.

[20] Guan L, Tang C, Yang K, Mo J, Huang Z. Effect of di-n-butyl ether blending with soybean-biodiesel on spray and atomization characteristics in a common-rail fuel injection system. Fuel 2015;140:116–25. https://doi.org/10.1016/j.fuel.2014.09.104.

[21] Gao Z, Zhu L, Zou X, Liu C, Tian B, Huang Z. Soot reduction effects of dibutyl ether (DBE) addition to a biodiesel surrogate in laminar coflow diffusion flames. Proc Combust Inst 2019;37:1265–72. https://doi.org/10.1016/j.proci.2018.05.083.

[22] Fu W, Li F, Zhang H, Yi B, Liu Y, Lin Q. Liftoff behaviors and flame structure of dimethyl ether jet flame in CH4/air vitiated coflow. Proc Inst Mech Eng Part A J Power Energy 2019;233:1039–46. https://doi.org/10.1177/0957650919846007.

[23] Yang J, Lim O. An investigation of the spray characteristics of diesel-DME blended fuel with variation of ambient pressure in a constant volume combustion chamber. J Mech Sci Technol 2014;28:2363–8. https://doi.org/10.1007/s12206-014-0528-1.

[24] Attia AMA, Hassaneen AE. Influence of diesel fuel blended with biodiesel produced from waste cooking oil on diesel engine performance. Fuel 2016;167:316–28. https://doi.org/10.1016/j.fuel.2015.11.064.

[25] Ozkan S, Puna JF, Gomes JF, Cabrita T, Palmeira JV, Santos MT. Preliminary study on the use of biodiesel obtained from waste vegetable oils for blending with hydrotreated kerosene fossil fuel using calcium oxide (CaO) from natural waste materials as heterogeneous catalyst. Energies 2019:12. https://doi.org/10.3390/en12224306.

[26] Masoud SM, Attia AMA, Salem H, El-zoheiry RM. Investigation of jet A-1 and waste cooking oil biodiesel fuel blend flame characteristics stabilized by radial swirler in lean pre-vaporized premixed combustor. Energy 2023;263:125830. https://doi.org/10.1016/j.energy.2022.125830.

[27] El-Maghraby RM. A study on bio-diesel and jet fuel blending for the production of renewable aviation fuel. Mater Sci Forum 2020;1008 MSF:231–44. doi: 10.4028/www.scientific.net/MSF.1008.231.

[28] Saxena MC, Dubey P, Tripathi A. Surface tension of binary liquid mixture. Asian J Chem 2011;23:1411–2.

[29] Radwan Metwally Abd Elatif Elzoheiry. Investigation of Combustion Characteristics for Prevaporized Premixed Biofuel-Jet Mixtures A thesis submitted in partial fulfillment of the requirements of Investigation of Combustion Characteristics for Prevaporized Premixed Biofuel-Jet Mixtures. 2007.
[30] Çengel Ya. Thermodynamics: An Engineering Approach. 2004.
[31] Esta. Operating instructions. J Wildl Rehabil 2002;25:27.
[32] Malik MSA, Mohamad Shaiful AI, Mohd Ismail MS, Mohd Jaafar MN, Sahar AM. Combustion and emission characteristics of coconut-based biodiesel in a liquid fuel burner. Energies 2017;10:1–12. https://doi.org/10.3390/en10040458.
[33] Senthur Prabu S, Asokan MA, Roy R, Francis S, Sreelekh MK. Performance, combustion and emission characteristics of diesel engine fuelled with waste cooking oil bio-diesel/diesel blends with additives. Energy 2017;122:638–48. https://doi.org/10.1016/j.energy.2017.01.119.
[34] Kumar M, Tung Chong C, Karmakar S. Comparative assessment of combustion characteristics of limonene, Jet A-1 and blends in a swirl-stabilized combustor under the influence of pre-heated swirling air. Fuel 2022;316:123350. https://doi.org/10.1016/j.fuel.2022.123350.
[35] Attia AMA, Belal BY, El-Batsh HM, Moneib HA. Effect of waste cooking oil methyl ester – Jet A-1 fuel blends on emissions and combustion characteristics of a swirl-stabilized lean pre-vaporized premixed flame. Fuel 2020;267:117203. https://doi.org/10.1016/j.fuel.2020.117203.
[36] Venu H, Madhavan V. Influence of diethyl ether (DEE) addition in ethanol-biodiesel-diesel (EBD) and methanol-biodiesel-diesel (MBD) blends in a diesel engine. Fuel 2017;189:377–90. https://doi.org/10.1016/j.fuel.2016.10.101.
[37] Rakopoulos DC, Rakopoulos CD, Giakoumis EG, Dimaratos AM. Characteristics of performance and emissions in high-speed direct injection diesel engine fueled with diethyl ether/diesel fuel blends. Energy 2012;43:214–24. https://doi.org/10.1016/j.energy.2012.04.039.
[38] Arthur H. Lefebvre DRB. GAS turbine combustion: alternative fuels and emissions. 2010. doi: 10.1620/tjem.141.247.
[39] Lefebvre AH, Ballal DR. Gas turbine combustion: alternative fuels and emissions. CRC press; 2010.
[40] Johnson MR, Littlejohn D, Nazeer WA, Smith KO, Cheng RK. A comparison of the flowfields and emissions of high-swirl injectors and low-swirl injectors for lean premixed gas turbines. Proc Combust Inst 2005. https://doi.org/10.1016/j.proci.2004.07.040.
[41] El-Zoheiry RM, EL-Seesy AI, Attia AMA, He Z, El-Batsh HM. Combustion and emission characteristics of Jojoba biodiesel-jet A1 mixtures applying a lean premixed pre-vaporized combustion techniques: An experimental investigation. Renew Energy 2020;162:2227–45. doi: 10.1016/j.renene.2020.10.031.
[42] Blends B. Effects of diethyl ether introduction in emissions and performance of a diesel engine fueled with 2020:1–13.
[43] Palash SM, Kalam MA, Masjuki HH, Masum BM, Rizwanul Fattah IM, Mofijur M. Impacts of biodiesel combustion on NOx emissions and their reduction approaches. Renew Sustain Energy Rev 2013;23:473–90. https://doi.org/10.1016/j.rser.2013.03.003.
[44] Bridjesh P, Periyasamy P, Vijayarao A, Chaitanya K. MEA and DEE as additives on diesel engine using waste plastic oil diesel blends. Sustain Environ Res 2018;28:142–7. https://doi.org/10.1016/j.serj.2018.01.001.
[45] Smigins R, Zakis A. Impact of diethyl ether/rapeseed oil blends on performance and emissions of a light-duty diesel vehicle. Energies 2020:13. https://doi.org/10.3390/en13153788.
[46] Singh MS, Prabhahar PDM. Effect of diethyl ether on combustion and emission characteristics of biodiesel blend B20 algae oil. Int J Eng Adv Technol 2019;9(5609–14). https://doi.org/10.35940/ijeat.b3161.129219.
[47] Altaher MA, Andrews GE, Li H. Study of biodiesel emissions and carbon mitigation in gas turbine combustor 2014:290–8.
[48] Turns SR. An introduction to combustion concepts and applications. 3rd ed. 2012. doi: 10.1201/9780429158216-6.